DOI: 10.1002/mrm.29541

TECHNICAL NOTE

Magnetic Resonance in Medicine

Lung parenchyma transverse relaxation rates at 0.55 T

Bochao Li¹ | Nam G. Lee¹ | Sophia X. Cui² | Krishna S. Nayak^{1,3}

¹Department of Biomedical Engineering, Viterbi School of Engineering, University of Southern California, California Los Angeles, USA

²Siemens Medical Solutions USA, Los Angeles, California USA

³Ming Hsieh Department of Electrical and Computer Engineering, Viterbi School of Engineering, University of Southern California, California Los Angeles, USA

Correspondence

Bochao Li, MS, 3740 McClintock Ave, EEB 416, University of Southern California, Los Angeles, CA 90089-2564, USA. Email: bochaoli@usc.edu

Funding information

National Science Foundation, Grant/Award Number: 1828736 **Purpose:** To determine R_2 and R'_2 transverse relaxation rates in healthy lung parenchyma at 0.55 T. This is important in that it informs the design and optimization of new imaging methods for 0.55T lung MRI.

Methods: Experiments were performed in 3 healthy adult volunteers on a prototype whole-body 0.55T MRI, using a custom free-breathing electrocardiogram-triggered, single-slice echo-shifted multi-echo spin echo (ES-MCSE) pulse sequence with respiratory navigation. Transverse relaxation rates R_2 and R'_2 and off-resonance Δf were jointly estimated using nonlinear least-squares estimation. These measurements were compared against R_2 estimates from T₂-prepared balanced SSFP (T₂-Prep bSSFP) and R₂* estimates from multi-echo gradient echo, which are used widely but prone to error due to different subvoxel weighting.

Results: The mean R_2 and R_2' values of lung parenchyma obtained from ES-MCSE were 17.3 ± 0.7 Hz and 127.5 ± 16.4 Hz ($T_2 = 61.6 \pm 1.7$ ms; $T'_2 = 9.5 \text{ ms} \pm 1.6 \text{ ms}$), respectively. The off-resonance estimates ranged from -60to 30 Hz. The R_2 from T_2 -Prep bSSFP was 15.7 \pm 1.7 Hz (T_2 = 68.6 \pm 8.6 ms) and R_2^* from multi-echo gradient echo was 131.2 ± 30.4 Hz ($T_2^* = 8.0 \pm 2.5$ ms). Paired t-test indicated that there is a significant difference between the proposed and reference methods (p < 0.05). The mean R_2 estimate from T_2 -Prep bSSFP was slightly smaller than that from ES-MCSE, whereas the mean R'_2 and R^*_2 estimates from ES-MCSE and multi-echo gradient echo were similar to each other across all subjects.

Conclusions: Joint estimation of transverse relaxation rates and off-resonance is feasible at 0.55 T with a free-breathing electrocardiogram-gated and navigator-gated ES-MCSE sequence. At 0.55 T, the mean R_2 of 17.3 Hz is similar to the reported mean R_2 of 16.7 Hz at 1.5 T, but the mean R_2' of 127.5 Hz is about 5–10 times smaller than that reported at 1.5 T.

KEYWORDS

0.55T MRI, echo-shifted multi-echo spin echo, low-field MRI, lung imaging, transverse relaxation rates, R_2 and R_2' mapping

Preliminary versions of this work were presented at the ISMRM Workshop on Low Field MRI (March 2022) and at the ISMRM 30th Scientific Sessions (May 2022; Abstract #3372).

This is an open access article under the terms of the Creative Commons Attribution-NonCommercial License, which permits use, distribution and reproduction in any medium, provided the original work is properly cited and is not used for commercial purposes.

© 2022 The Authors. Magnetic Resonance in Medicine published by Wiley Periodicals LLC on behalf of International Society for Magnetic Resonance in Medicine.

1522 wileyonlinelibrary.com/journal/mrm Magn Reson Med. 2023;89:1522-1530.

1 | INTRODUCTION

Contemporary 0.55T MRI has provided the opportunity to evaluate lung anatomy and function with excellent image quality, largely due to reduced magnetic susceptibility, 1,2 smaller R_2 , and R_2^* . The small T_2^* , for example, opens exciting new opportunities such as long-readout (5–10 R) stack-of-spiral data sampling. Additionally, at conventional field strengths such as 3 T, it has been shown that the effective transverse relaxation rate R_2^* is valuable in characterizing smoking-related chronic obstructive pulmonary disease, and variations in R_2 may provide different pathological states of interstitial lung disease. Therefore, measurements of transverse relaxation rates are beneficial for MR pulse-sequence design, optimizing sequence parameters, and may have diagnostic value.

The irreversible transverse rate R_2 is typically estimated from spin-echo pulse sequences or a T₂-prepared balanced SSFP (T2-Prep bSSFP)7 pulse sequence, while the effective transverse relaxation rate R_2^* is typically estimated from multi-echo gradient-echo (ME-GRE) pulse sequences.^{8,9} Initial measurements of lung parenchyma R_2 and R_2^* at 0.55 T were reported.³ The reversible transverse relaxation rate R'_{2} can be calculated from separately estimated R_2 and R_2^* using two different pulse sequences. However, the resultant R'_2 estimate could be biased because (1) signal generating mechanisms are inherently different in two pulse sequences^{10,11}; for example, a spin-echo pulse sequence inherently suppresses flowing blood known as "washout" effect¹²; (2) assumptions made for deriving an analytic signal model for each R_2 and R_2^* mapping may not be identical; and (3) variance in each parameter estimate can be different due to the difference in signal-to-noise ratio (SNR) of R_2 and R_2^* mapping.

In this work, we perform concurrent measurements of the irreversible (thermodynamics) and reversible (field inhomogeneity) transverse relaxation rates¹³ (R_2 and R'_2) of lung parenchyma using a free-breathing electrocardiogram (ECG)-gated and navigator-gated single-slice echo-shifted multi-echo spin-echo (ES-MCSE) sequence. Using a single pulse sequence for estimating several parameters of interest is beneficial, as only one imaging parameter relevant to a signal model can be changed at a time (e.g., echo time shift), with the rest of imaging parameters fixed throughout the scan. Physiological noise due to cardiac and respiratory motion can be consistent; hence, noise levels of all scans can be identical. Direct R'_2 estimation from the single ES-MCSE sequence could avoid bias resulting from the effects mentioned previously in separate R_2 and R_2^* mapping. Our results indicate that R_2 and R_2' estimates are consistent with those from a previous report.3

2 | METHODS

2.1 | Acquisition

Experiments were performed using a whole-body 0.55T system (prototype MAGNETOM Aera; Siemens Healthineers, Erlangen, Germany) equipped with high-performance shielded gradients (45 mT/m amplitude, 200T/m/s slew rate). The integrated body coil was used for RF transmission. A six-element body coil (anterior) and six elements from an 18-element spine coil (posterior) were used for signal reception. The scanner's default shimming setting (tune-up mode) was used for both shimming and center-frequency determination for all subjects. Three healthy volunteers (2 males/1 female, ages 24–31) were scanned under a protocol approved by our institutional review board after providing written informed consent.

Figure 1 illustrates the proposed free-breathing, ECG-triggered, and respiratory-gated ES-MCSE pulse sequence. The proposed sequence performed a segmented k-space acquisition for each echo shift. For a given phase-encoding step, eight readouts were acquired at middiastole and end-expiratory respiratory phase. Subsequently, eight readouts for the next phase-encoding step were acquired during an RR interval at end-expiratory phase, repeating until the last echo shift. The range of spin echo times (t_{SE}) were 20, 40, 60, 80, 100, 120, 140, and 160 ms to capture T₂ decay. The readout gradient and ADC were shifted within the given echo spacing (20 ms) (ie, the time interval between two consecutive refocusing pulses). The negative and positive echo shifts, t_{shift} , captured the rephasing and dephasing portions of signal evolution. The range of echo shifts were -4, -2, 0, 2, and 4 ms to take full advantage of the echo spacing while avoiding overlapping between the ramps of a shifted readout with the plateau of a slice-selection gradient. All five echo shifts were measured in one single scan so that spatial registration across images was not required. Fast gradient and RF modes were selected to maximize the time interval between refocusing pulses and gradients. The phase-encoding direction was selected from right to left on a coronal plane. Siemens' navigator-triggered prospective acquisition correction¹⁴ was used to mitigate respiratory motion, and data acquisition was performed at the end-expiratory phase. Phase oversampling was not used. The total scan time was 40 min for coronal orientation and 16 min for sagittal orientation. Sagittal scans required fewer phase-encode steps due to the smaller FOV in anterior-posterior direction.

For comparison, inline R_2 and R_2^* mapping based on product T_2 -Prep bSSFP and ME-GRE pulse sequences were performed using the parameters modified based on Campbell-Washburn et al.³ The T_2 -Prep bSSFP and ME-GRE were breath-hold scans at end-expiratory phase,

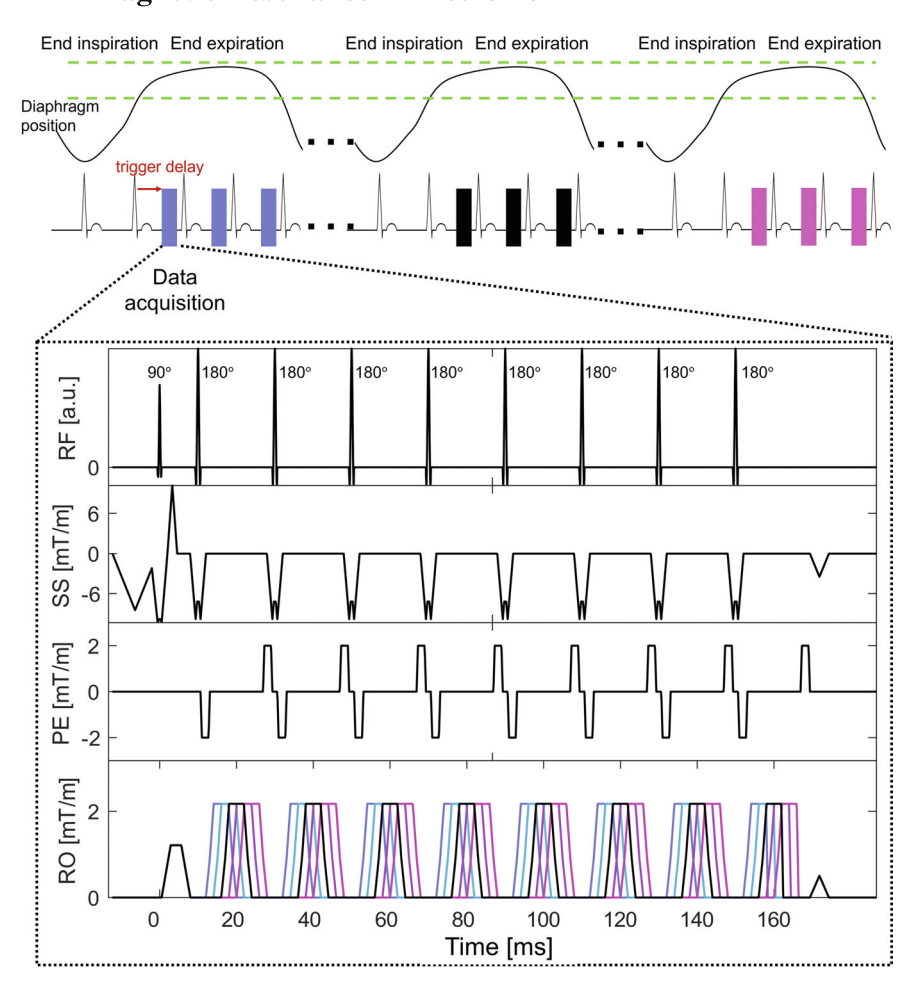


FIGURE 1 Illustration of a free-breathing electrocardiogram (ECG)-triggered and respiratory-gated single-slice echo-shifted multi-echo spin echo (ES-MCSE). A diaphragm motion curve indicates various respiratory phases. The acceptance window of a respiratory motion navigator is chosen at end-expiratory phase, and ECG triggering is used to acquire data at end-diastole with a trigger delay time. An imaging module consists of eight readouts per phase-encoding step, and five echo shifts (-4, -2, 0, 2,and 4 ms) are demonstrated with shifted readout gradients in different colors. Abbreviations: PE, phase-encoding; RO, readout; SS, single slice

while ECG triggering was only used for T_2 -Prep bSSFP. Note that a free-breathing ME-GRE technique 15 has been developed but we did not use this technique in our study. Parallel imaging was not adapted in any sequence. All scans used a FOV of 360×360 mm, a slice thickness of 5 mm, an in-plane spatial resolution of 2.8×2.8 mm², a reconstruction matrix of 128×128 , and a phase oversampling of 15% to avoid aliasing. The imaging parameters are listed in Supporting Table S1 and summarized here:

- ES-MCSE (ECG-triggered; free breathing at endexpiratory phase)
 - $t_{\text{SE}} = 20, 40, 60, 80, 100, 120, 140,$ and 160 ms; TR = 250 ms
 - · 260 Hz/pixel bandwidth
 - excitation flip angle = 90° ; refocusing flip angle = 180°
 - 40-min (coronal), 16-min (sagittal) acquisition time
- T₂-Prep bSSFP (ECG-triggered; breath-hold a end-expiratory phase)
 - preparation time $T_{\text{prep}} = 0, 5, 25, \text{ and } 55 \text{ ms}$

- TE/TR = 1.09/192 ms
- · 1184 Hz/pixel bandwidth
- excitation flip angle = 70°
- 9-s acquisition time
- ME-GRE (non-ECG triggered; breath-hold at endexpiratory phase)
 - TE = 1.8, 4.6, 7.4, and 10.2 ms; TR = 361.5 ms
 - 590 Hz/pixel bandwidth
 - excitation flip angle = 15°
 - 24-s acquisition time

2.2 Relaxation-rate constant estimation

A 2D Gaussian smoothing filter ($\sigma=1$) was applied to the complex-valued ES-MCSE images before parameter estimation. Due to stimulated echo contamination in MCSE and phase shifts of moving spins, the first spin echo (all five echo shifts) were discarded to improve the accuracy of T_2 quantification. 16,17 A total of 35 complex images (7 spin-echo times \times 5 echo shifts) were used for parameter estimation. We used a three-parameter complex signal

model based on ideal 180° refocusing pulses for simultaneous R_2 , R'_2 , and Δf estimation. The signal evolutions for rephasing ($t_{\text{shift}} \leq 0$) and dephasing ($t_{\text{shift}} \geq 0$) portions of spin echoes, respectively, can be described as

$$S(\vec{r}, t_{\text{shift}}) = S_0 e^{-(t_{\text{SE}} + t_{\text{shift}})R_2(\vec{r}) + t_{\text{shift}}R'_2(\vec{r})} e^{-j2\pi\Delta f(\vec{r})t_{\text{shift}}}$$

$$\text{for } t_{\text{shift}} \le 0$$

$$S(\vec{r}, t_{\text{shift}}) = S_0 e^{-(t_{\text{SE}} + t_{\text{shift}})R_2(\vec{r}) - t_{\text{shift}}R'_2(\vec{r})} e^{-j2\pi\Delta f(\vec{r})t_{\text{shift}}}$$

$$\text{for } t_{\text{shift}} > 0 \tag{1}$$

where S $(\vec{r},t_{\text{shift}}) \in \mathbb{C}$ denotes the complex-valued signal at position \vec{r} acquired at t_{shift} ; $S_0 \in \mathbb{C}$ denotes complex-valued spin magnetization; $R_2 \in \mathbb{R}$ and $R_2 \in \mathbb{R}$ denote real-valued irreversible and reversible transverse relaxation rates, respectively; and $\Delta f \in \mathbb{R}$ denotes static off-resonance. Seven spin echoes and five echo shifts were used. Parameter estimation was performed using a nonlinear least-squares approach with nonnegative real constraints on R_2 and R_2 , and real constraint on Δf . We also replicated the measurements of R_2 from T₂-Prep bSSFP and R_2 from ME-GRE with reasonable modification of the protocol by Campbell-Washburn et al.³ The R_2 and R_2 maps were obtained by fitting a mono-exponential signal model for each pixel from T₂-Prep bSSFP and ME-GRE magnitude images:

$$S(\vec{r}, T_{\text{prep}}) = S_0 e^{-T_{\text{prep}} \cdot R_2}$$
 (2)

$$S(\vec{r}, TE) = S_0 e^{-TE \cdot R_2^*}$$
 (3)

where T_{prep} is the preparation time for T_2 -Prep bSSFP, and TE is the echo time for ME-GRE.

2.3 | Numerical simulation

To analyze the sensitivity of the chosen t_{SE} and t_{shift} to the range of R_2 and R_2' in lung, we performed numerical simulations for the anticipated ranges of R_2 (14–20 Hz), R_2' (60–110 Hz), and Δf (–30 to 30 Hz). An EC-MCSE signal with a perfect refocusing pulse as described in Equation (1) was used to generate a noiseless signal evolution. A total of 35 samples excluding the first TE (7 spin echo times × 5 echo shifts) was simulated using the same echo shifts and spin echo times as the in vivo scan. We measured realistic SNR in lung from an in vivo image ($t_{SE} = 40$ ms) with the following equation:

$$SNR = \frac{S}{\sigma}$$
,

where S is the mean value of signal intensity over a region of interest (ROI) in lung and σ is the SD over an ROI

in image background.¹⁸ An SNR of 18 was simulated by adding independent and identically distributed complex Gaussian noise¹⁹ to the noiseless ES-MCSE signal. For a given set of R_2 , R'_2 and Δf , estimated R_2 , R'_2 , and Δf were computed for each of 10 000 noise realizations. The bias and SD of estimated R_2 , R'_2 , and Δf were then calculated. Simulated and in vivo data were processed identically.

2.4 | Data analysis

Lung ROIs excluding heart, spine, and external structures were manually drawn from the anatomical images and applied on each parameter map. A conservative mask was generated by excluding boundaries of the lung to avoid motion-induced blurring effects. The spatial mean and spatial SD within the lung ROIs were reported for each subject. A paired t-test was performed to determine the statistical difference among different mapping methods.

The within-ROI SD for the *i*th subject is defined as $\sigma_j = \sqrt{\frac{\sum_{k=1}^{K_i} (y_{k,l} - \bar{y}_i)^2}{K_i - 1}}$, where k is the index of a voxel in an ROI; y_k is the estimated parameter for the kth voxel; K_i is the number of voxels in an ROI for the subject; and \bar{y}_i is the mean within an ROI for the subject.

Let BMS and WMS be the between-subject means of squares and within-subject means-of-squares for 3 subjects, defined as follows:

BMS =
$$\frac{\sum_{i=1}^{3} K_i (\bar{y}_i - \bar{y})^2}{3}$$
 (4)

WMS =
$$\frac{\sum_{i=1}^{3} \sum_{k=1}^{K_{i}} (y_{k,i} - \bar{y}_{i})^{2}}{\sum_{i=1}^{3} (K_{i} - 1)},$$
 (5)

where \bar{y} is the mean of all voxels from all 3 subjects. Then the between-subject SD σ_b is defined as²⁰

$$\sigma_b = \sqrt{\frac{(BMS - WMS)}{\min(K_1, K_2, K_3)}}.$$
 (6)

3 | RESULTS

Figure 2 shows two representative examples of a simulated signal evolution and an estimated signal evolution: (1) $R_2/R_2' = 14/60\,\text{Hz}$ and (2) $R_2/R_2' = 20/110\,\text{Hz}$ with Δf of 0. Estimated R_2 and R_2' bias was < 0.03 and 0.5 Hz, respectively, across the simulated parameter ranges and considered negligible. Figure 2C,D illustrates the aggregate SD of R_2 and R_2' for each pair of ground-truth R_2 and

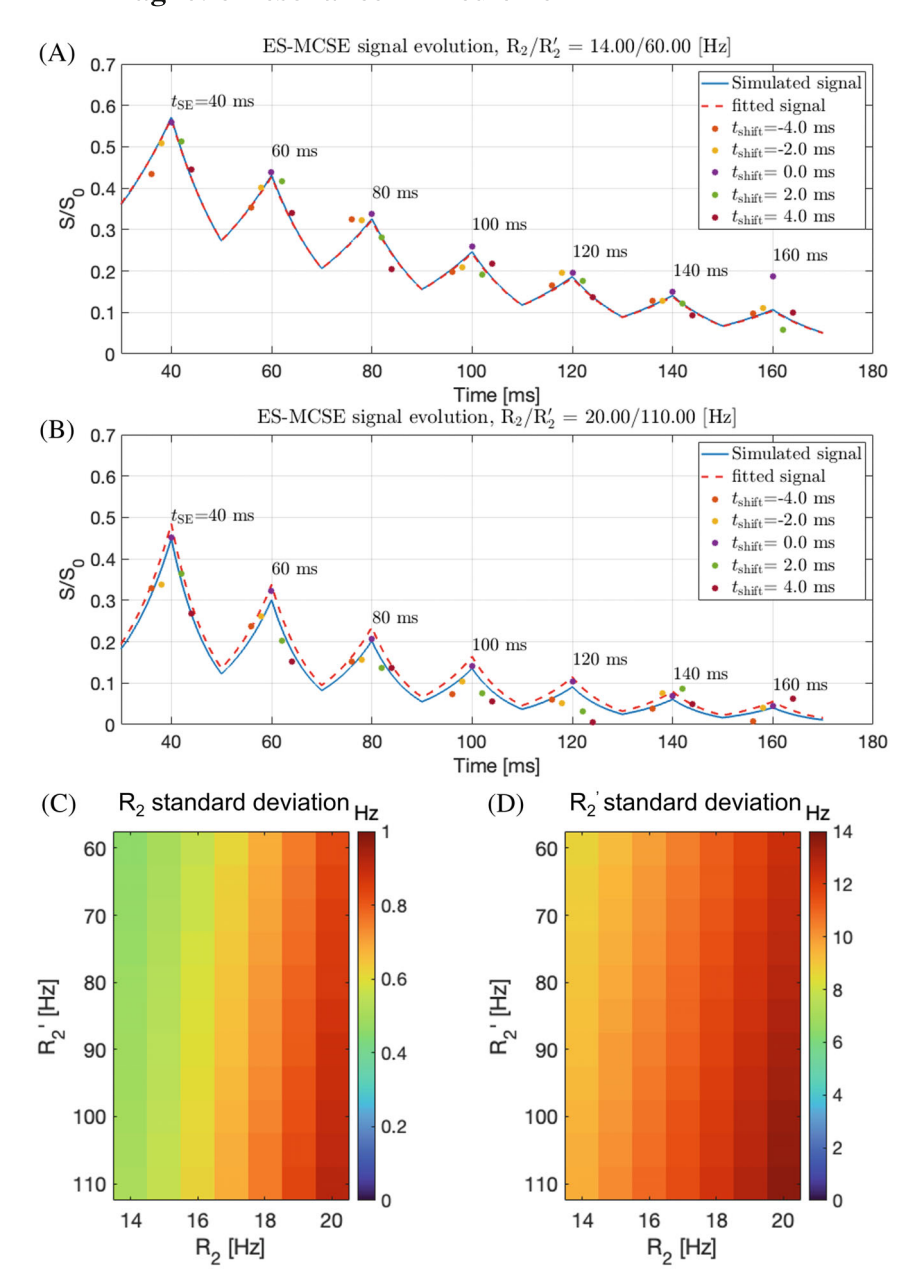


FIGURE 2 Estimated signal evolutions are shown for two representative on-resonance cases: $R_2/R_2' = 14/60\,\mathrm{Hz}\,(\mathrm{A})$ and $20/110\,\mathrm{Hz}\,(\mathrm{B})$. Standard of R_2 and R_2' estimates from ES-MCSE using seven spin echo times and five echo shifts. A simulated noiseless signal evolution (blue), noisy samples (dots in different colors), and the aggregate SD of R_2 (C) and R_2' (D) for a pair of R_2 and R_2' are calculated from 10 000 noise realizations across all Δf from -30 to $30\,\mathrm{Hz}$

 R'_2 across all Δf from -30 to 30 Hz. Larger SD of both parameters occurs at large R_2 values. Figure 3 illustrates voxel-wise parameter estimation from a total of 35 complex images (7 spin echo times \times 5 echo shifts).

Table 1 summarizes the results from 3 volunteers obtained with ES-MCSE and reference methods. For the ES-MCSE method, the mean and intersubject SD of R_2 estimates of lung parenchyma was $17.3 \pm 0.7 \, \text{Hz}$ ($T_2 = 61.1 \pm 1.7 \, \text{ms}$), and similar to that reported at $1.5 \, \text{T.}^{21}$ The mean and intersubject SD of R_2' estimates was approximately $127.5 \pm 16.4 \, \text{Hz}$ ($T_2' = 9.5 \pm 1.6 \, \text{ms}$), and the calculated mean and intersubject SD of R_2^* estimates was approximately $144.8 \pm 16.7 \, \text{Hz}$ ($T_2^* = 8.2 \pm 2.4 \, \text{ms}$), which is about 5–10 times smaller than that reported at 1.5 $T.^{3,22,23}$ The mean R_2 estimate from ES-MCSE is slightly smaller than that from T_2 -Prep bSSFP ($R_2 = 15.7 \pm 1.7 \, \text{Hz}$;

 $T_2 = 68.6 \pm 8.6 \,\mathrm{ms}$), and ES-MCSE provides a smaller variance of R_2 estimates compared with T_2 -Prep bSSFP. A t-test was performed on all 3 subjects, and indicates that there is a significant difference in R_2 estimates from ES-MCSE and T₂-Prep bSSFP (p < 0.05). A smaller R₂ estimate from T₂-Prep bSSFP may be due to the mixed T₁/T₂ contrast of bSSFP, as indicated by the previous work about the underestimation of R_2 .^{24,25} The ES-MCSE technique provides a smaller variance of R_2^* estimates compared with that from ME-GRE ($R_2^* = 131.2 \pm 30.4 \,\mathrm{Hz}$; $T_2^* = 8.0 \pm 2.5$ ms). The R_2^* and R_2' results in Table 1 show a discrepancy between ES-MCSE and reference methods within a subject, whereas the values are consistent in the whole subject group level. The within-subject discrepancy may be due to the use of a different motion-compensating strategy.

FIGURE 3 Representative ES-MCSE images of seven spin echo times and five echo shifts. The images at the first TE (20 ms) were discarded (not shown) due to stimulated-echo contamination. A signal evolution of 35 samples was used for pixelwise parameter estimation to yield R_2 and R_2' maps

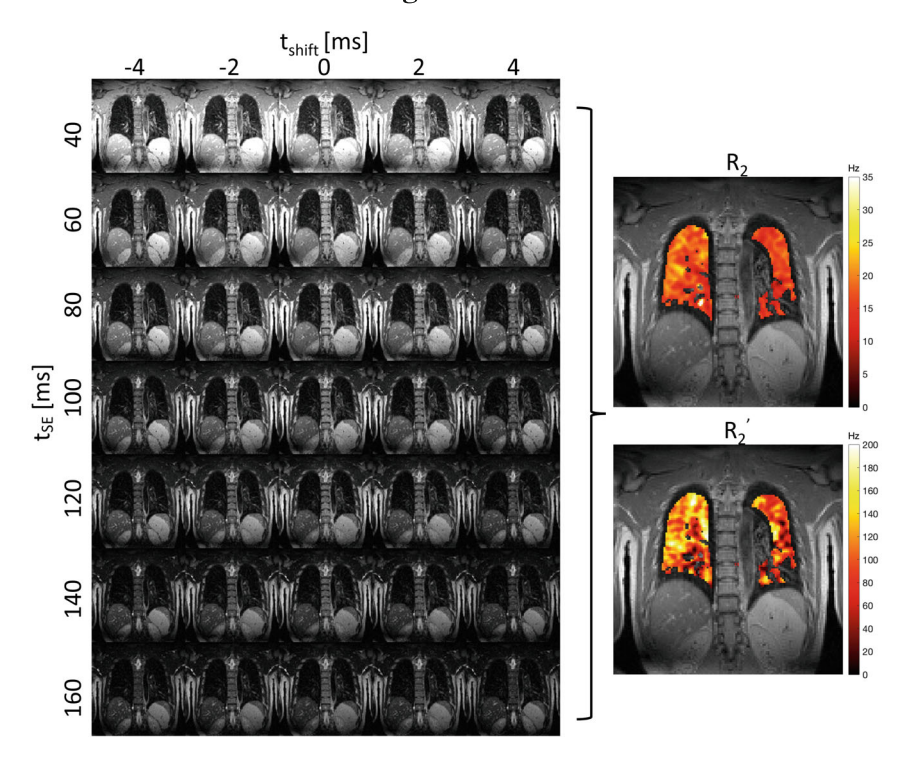


TABLE 1 Summary results for measured R_2 and R_2' from 3 healthy volunteers (within–region-of-interest mean \pm SD for each subject and intersubject mean \pm SD in the last row)

	ES-MCSE			Reference methods		
Subject	R_2 (Hz)	R' ₂ (Hz)	R_2^* (Hz)	R_2 (Hz)	R_2' (Hz)	R_2^* (Hz)
S1	16.7 ± 4.4	103.9 ± 38.8	120.5 ± 39.7	15.6 ± 3.2	153.9 ± 45.9	169.5 ± 47.7
S2	17.0 ± 3.5	139.9 ± 41.3	156.9 ± 42.1	14.1 ± 3.9	88.4 ± 31.8	102.5 ± 32.0
S3	17.9 ± 4.5	130.0 ± 58.1	148.5 ± 59.5	17.5 ± 3.5	118.2 ± 41.8	135.7 ± 43.0
All	17.3 ± 0.7	127.5 ± 16.4	144.8 ± 16.7	15.7 ± 1.7	115.5 ± 29.6	131.2 ± 30.4

Note: The first three columns show the results from ES-MCSE. The R_2^* from ES-MCSE is calculated by $R_2^* = R_2 + R_2'$. The last three columns show the results from reference methods. The R_2' from reference methods is calculated by $R_2' = R_2^* - R_2$, where R_2 and R_2^* are measured from T_2 -prepared balanced SSFP and multi-echo gradient echo, respectively.

Figure 4 shows the R_2 , R'_2 , and off-resonance maps for 3 healthy subjects. For each subject, the R_2 map was more homogeneous compared with the R'_2 map. The regional difference between lung parenchymal resonant frequency and the scan center frequency, simultaneously estimated from ES-MCSE, ranged from $-60 \, \text{Hz}$ to $30 \, \text{Hz}$ after shimming and center frequency determination using the scanner's default ("tune-up") preparatory calibration. Supporting Information Figure S1 shows the histograms of the off-resonance within ROIs for all 3 subjects.

4 | DISCUSSION

The proposed single-sequence approach was able to estimate R_2 , R'_2 , and Δf simultaneously and produced results

comparable to those reported from the previous study. The R_2' estimate from the proposed ES-MCSE method shows less intersubject variance with higher precision than that from the reference methods. Note that the measurements were acquired on one single coronal slice that intersects the center of the descending aorta, and the different slices may result in different measurements due to gravitation dependence of lung water distribution.²⁶

The ranges of R_2 and R_2' (or R_2^*) are decreased at low field; this allows flexibility in pulse sequence design, including a longer readout in spiral imaging, in multi-echo imaging, and in non-Cartesian bSSFP imaging. With a smaller R_2^* value at 0.55 T, a longer readout time up to 10 ms could be used to further improve imaging efficiency. The proposed method can potentially be used in other applications, such as liver T_2' mapping

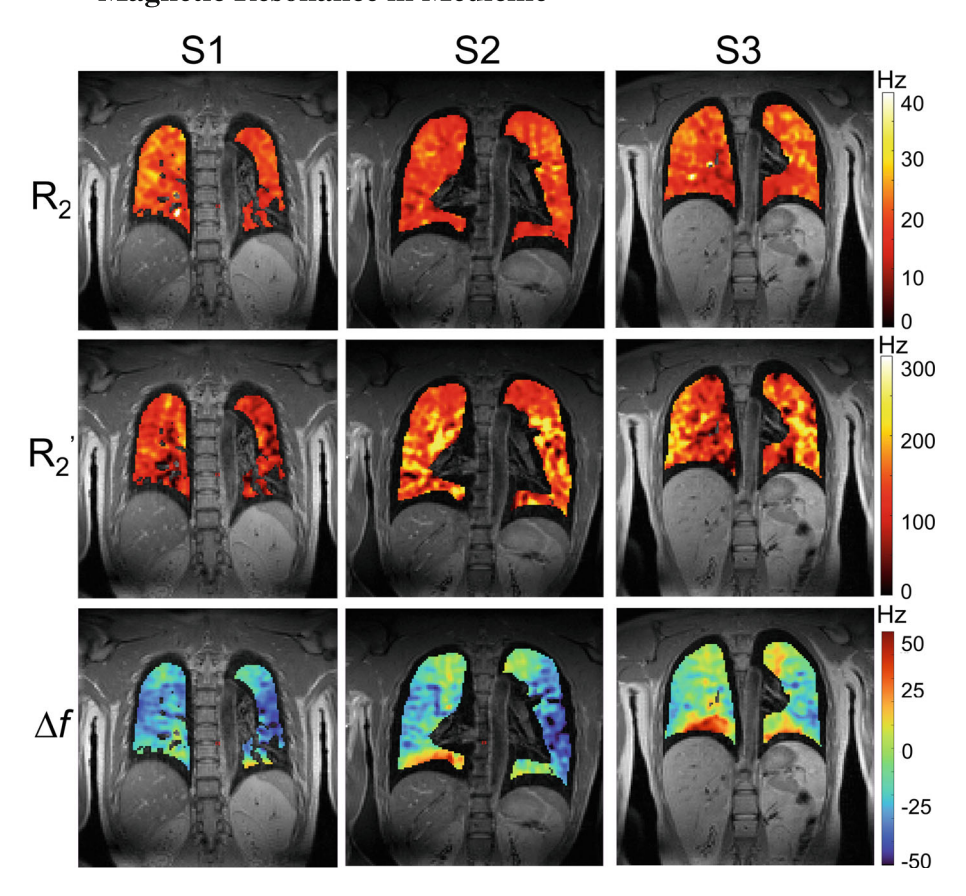


FIGURE 4 In vivo parameter maps estimated from ES-MCSE. The R_2 , R'_2 , and Δf maps within region of interests for 3 healthy subjects were estimated from EC-MCSE. Images were acquired at middiastole and end-expiratory phase, and of a coronal slice that intersects the descending aorta

and intramyocardial hemorrhage quantification. 27,28 The investigation of transverse time constants on lung disease 29 can potentially be used to infer different pathological features. However, the accuracy of R_2' and R_2^* still needs to be further improved, overcoming the current limitations.

First, a long acquisition time (40–45 min) of ES-MCSE could be accelerated with parallel imaging with compressed sensing 30 or an advanced reconstruction method based on subspace modeling such as $\rm T_2$ shuffling 31 and echo planar time-resolved imaging. 32 Second, the assumption of perfect $\rm B_1^+$ homogeneity in the signal model may lead to bias in quantification. Advanced signal modeling incorporating $\rm B_1^+$ inhomogeneity could result in improved quantification. 33,34

The measurements reported in this paper are vulnerable to partial volume effects with the designed in-plane resolution of 2.8×2.8 mm². Although we seek to measure lung parenchyma only, there is contribution from blood in the capillaries and small blood vessels such as segmental/subsegmental arteries and veins. The bias of T_2 with limited in-plane resolution have been found due to partial volume effects,³⁵ and the apparent R_2 may be smaller in lung parenchyma, which is contaminated from smaller blood R_2 . Additionally, because pulmonary arterial blood is deoxygenated and venous blood is oxygenated, they may exert different effects on the measurement of R_2^* and R_2' in

the one voxel, depending on the distribution of these blood vessels.

5 | CONCLUSIONS

We demonstrate the feasibility of ES-MCSE to jointly estimate R_2 , R_2' , and off-resonance at 0.55 T. The results shows that the mean R_2 estimate of 17.3 Hz is similar to that at 1.5 T,²¹ and the mean R_2' estimate of 127.5 Hz (mean R_2^* estimate of 144.8 Hz) is 5–10 times smaller than those at 1.5 T.^{23,36} Additionally, off-resonance in lung parenchyma ranges from -60 to $30\,\mathrm{Hz}$ at 0.55 T.

ACKNOWLEDGMENT

This work was supported by the National Science Foundation (#1828763). We also receive research support from Siemens Healthineers.

CONFLICT OF INTEREST

Sophia Cui is an employee of Siemens Healthineers.

DATA AVAILABILITY STATEMENT

The code and sample data that support the findings of this study are openly available in GitHub at https://github.com/usc-mrel/LowField-ESMCSE.git.

ORCID

Bochao Li https://orcid.org/0000-0002-5267-9129
Nam G. Lee https://orcid.org/0000-0001-5462-1492
Sophia X. Cui https://orcid.org/0000-0002-5133-4903
Krishna S. Nayak https://orcid.org/0000-0001-5735-3550

REFERENCES

- Bhattacharya I, Ramasawmy R, Javed A, et al. Oxygen-enhanced functional lung imaging using a contemporary 0.55 T MRI system. NMR Biomed. 2021;34:1-10.
- Campbell-Washburn AE, Bhattacharya I, Moss J, et al. T2-weighted lung parenchymal imaging using a high-performance low field MRI system. Am J Resp Crit Care Med. 2020;201:A3250.
- Campbell-Washburn AE, Ramasawmy R, Restivo MC, et al. Opportunities in interventional and diagnostic imaging by using high-performance low-field-strength MRI. *Radiology*. 2019;293:384-393.
- 4. Javed A, Ramasawmy R, Moss J, et al. Optimized 3D spiral ultra-short echo time free-breathing pulmonary imaging on a high-performance low-field 0.55T scanner. In: Proceedings of the 29th Annual Meeting of ISMRM [Virtual], 2021. Abstract #596.
- Ohno Y, Koyama H, Yoshikawa T, et al. T₂* measurements of 3-T MRI with ultrashort TEs: capabilities of pulmonary function assessment and clinical stage classification in smokers. *Am J Roentgenol.* 2011;197:279-285.
- Buzan MTA, Eichinger M, Kreuter M, et al. T2 mapping of CT remodelling patterns in interstitial lung disease. *Eur Radiol*. 2015;25:3167-3174.
- Nezafat R, Stuber M, Ouwerkerk R, Gharib AM, Desai MY, Pettigrew RI. B1-insensitive T2 preparation for improved coronary magnetic resonance angiography at 3 T. Magn Reson Med. 2006;55:858-864.
- 8. Hatabu H, Alsop DC, Listerud J, Bonnet M, Gefter WB. T₂* and proton density measurement of normal human lung parenchyma using submillisecond echo time gradient echo magnetic resonance imaging. *Eur J Radiol.* 1999;29:245-252.
- 9. Pracht ED, Arnold JFT, Wang T, Jakob PM. Oxygen-enhanced proton imaging of the human lung using T_2^* . *Magn Reson Med.* 2005;53:1193-1196.
- 10. Chavhan GB, Babyn PS, Jankharia BG, Cheng HLM, Shroff MM. Steady-state MR imaging sequences: physics, classification, and clinical applications. *Radiographics*. 2008;28:1147-1160.
- 11. Kacere RD, Pereyra M, Nemeth MA, Muthupillai R, Flamm SD. Quantitative assessment of left ventricular function: steady-state free precession MR imaging with or without sensitivity encoding. *Radiology*. 2005;235:1031-1035.
- Plein S, Greenwood J, Ridgway JP. Cardiovascular MR Manual. Berlin, Germany: Springer Nature; 2011.
- 13. Ma J, Wehrli FW. Method for image-based measurement of the reversible and irreversible contribution to the transverse-relaxation rate. *J Magn Reson B.* 1996;111:61-69.
- Thesen S, Heid O, Mueller E, Schad LR. Prospective acquisition correction for head motion with image-based tracking for real-time fMRI. Magn Reson Med. 2000;44:457-465.

- Kellman P, Bandettini WP, Mancini C, Hammer-Hansen S, Hansen MS, Arai AE. Characterization of myocardial T1-mapping bias caused by intramyocardial fat in inversion recovery and saturation recovery techniques. *J Cardiovasc Magn Reson*. 2015;17:33.
- Maier CF, Tan SG, Hariharan H, Potter HG. T2 quantitation of articular cartilage at 1.5 T. J Magn Reson Imaging. 2003;17:358-364.
- 17. Axel L. Blood flow effects in magnetic resonance imaging. *Am J Roentgenol.* 1984;143:1157-1166.
- Dietrich O, Raya JG, Reeder SB, Reiser MF, Schoenberg SO. Measurement of signal-to-noise ratios in MR images: influence of multichannel coils, parallel imaging, and reconstruction filters. J Magn Reson Imaging. 2007;26:375-385.
- Wilkins B, Lee N, Gajawelli N, Law M, Leporé N. Fiber estimation and tractography in diffusion MRI: development of simulated brain images and comparison of multi-fiber analysis methods at clinical b-values. *Neuroimage*. 2015;109:341-356.
- 20. Barnhart HX, Barboriak DP. Applications of the repeatability of quantitative imaging biomarkers: a review of statistical analysis of repeat data sets. *Transl Oncol.* 2009;2:231-235.
- Bauman G, Santini F, Pusterla O, Bieri O. Pulmonary relaxometry with inversion recovery ultra-fast steady-state free precession at 1.5T. Magn Reson Med. 2017;77:74-82.
- 22. Wild JM, Marshall H, Bock M, et al. MRI of the lung (1/3): methods. *Insights Imaging*. 2012;3:345-353.
- 23. Yu J, Xue Y, Song HK. Comparison of lung T_2^* during free-breathing at 1.5 T and 3.0 T with ultrashort echo time imaging: lung T_2^* measurements at 1.5 T and 3.0 T with UTE. *Magn Reson Med.* 2011;66:248-254.
- 24. Guo R, Cai X, Kucukseymen S, et al. Free-breathing simultaneous myocardial T₁ and T₂ mapping with whole left ventricle coverage. *Magn Reson Med.* 2021;85:1308-1321.
- 25. Baeßler B, Schaarschmidt F, Stehning C, Schnackenburg B, Maintz D, Bunck AC. Cardiac T2-mapping using a fast gradient echo spin echo sequence—first in vitro and in vivo experience. *J Cardiovasc Magn Reson*. 2015;17:67.
- Seemann F, Javed A, Chae R, et al. Imaging gravity-induced lung water redistribution with automated inline processing at 0.55 T cardiovascular magnetic resonance. *J Cardiovasc Magn Reson*. 2022;24:35.
- 27. Wood JC, Enriquez C, Ghugre N, et al. MRI R_2 and R_2^* mapping accurately estimates hepatic iron concentration in transfusion-dependent thalassemia and sickle cell disease patients. *Blood.* 2005;106:1460-1465.
- Rossello X, Lopez-Ayala P, Fernández-Jiménez R, et al. R2 prime (R20) magnetic resonance imaging for post-myocardial infarction intramyocardial haemorrhage quantification. Eur Heart J Cardiovasc Imaging. 2020;21:1031-1038.
- Bergin CJ, Glover GH, Pauly JM. Lung parenchyma: magnetic susceptibility in MR imaging. *Radiology*. 1991;180:845-848.
- Lustig M, Donoho D, Pauly JM. Sparse MRI: the application of compressed sensing for rapid MR imaging. *Magn Reson Med*. 2007;58:1182-1195.
- 31. Tamir JI, Uecker M, Chen W, et al. T₂ shuffling: sharp, multicontrast, volumetric fast spin-echo imaging. *Magn Reson Med.* 2017;77:180-195.
- 32. Dong Z, Wang F, Reese TG, Bilgic B, Setsompop K. Echo planar time-resolved imaging with subspace reconstruction

- and optimized spatiotemporal encoding. *Magn Reson Med.* 2020;84:2442-2455.
- 33. Chhetri G, McPhee KC, Wilman AH. Bloch modelling enables robust T2 mapping using retrospective proton density and T2-weighted images from different vendors and sites. *Neuroimage*. 2021;237:118116.
- 34. Lebel RM, Wilman AH. Transverse relaxometry with stimulated echo compensation. *Magn Reson Med.* 2010;64:1005-1014.
- Stainsby JA, Wright GA. Partial volume effects on vascularT2 measurements. Magn Reson Med. 1998;40:494-499.
- 36. Mulkern R, Haker S, Mamata H, et al. Lung parenchymal signal intensity in MRI: a technical review with educational aspirations regarding reversible versus irreversible transverse relaxation effects in common pulse sequences: lung parenchymal signal intensity In MRI. Concepts Magn Reson Part A. 2014;43A: 29-53.

SUPPORTING INFORMATION

Additional supporting information may be found in the online version of the article at the publisher's website.

Figure S1. Histograms of off-resonance in lung parenchyma for 3 subjects, estimated using the proposed echo-shifted multi-echo spin echo (ES-MCSE) sequence. All frequency values are relative to the scanner center frequency after default shimming (tune-up mode). The interquartile range (25th to 75th percentile) is colored orange.

Table S1. The ES-MCSE, T₂-prepared balanced SSFP, and multi-echo gradient-echo sequence parameters

Video S1. Scrolling through all 35 images (7 spin echo times × 5 echo shifts) for the S1 subjects. Notice the adequate spatial registration of all images, which were obtained in a single 40-min, free-breathing, electrocardiogram (ECG)–gated scan

Video S2. Scrolling through all 35 images (7 spin echo times × 5 echo shifts) for the S2 subjects. Notice the adequate spatial registration of all images, which were obtained in a single 40-min, free-breathing, ECG-gated scan

Video S3. Scrolling through all 35 images (7 spin echo times × 5 echo shifts) for the S3 subjects. Notice the adequate spatial registration of all images, which were obtained in a single 40-min, free-breathing, ECG-gated scan

How to cite this article: Li B, Lee NG, Cui SX, Nayak KS. Lung parenchyma transverse relaxation rates at 0.55 T. *Magn Reson Med*. 2023;89:1522-1530. doi: 10.1002/mrm.29541